Surface Science 617 (2013) 192–198

Contents lists available at ScienceDirect

Surface Science

journal homepage: www.elsevier.com/locate/susc

Alloy formation and chemisorption at Cu/Pt(111) bimetallic surfaces using alkali ISS, XPD, and TPD

Chih-Sung Ho [a], Santanu Banerjee [b], John P. Roszell [c], Bruce E. Koel [c,*]

[a] Department of Chemical and Materials Engineering, Tunghai University, Taichung 40704, Taiwan
[b] Department of Physics, Tougaloo College, Tougaloo, MS 39174, USA
[c] Department of Chemical and Biological Engineering, Princeton University, A311 Engineering Quad, Princeton, NJ 08540, USA

ARTICLE INFO

Article history:
Received 19 May 2013
Accepted 3 August 2013
Available online 14 August 2013

Keywords:
Copper
Platinum
Alloys
Alkali ion scattering
Temperature programmed desorption
X-ray photoelectron diffraction

ABSTRACT

Alloying and surface structures of Cu films evaporated onto a Pt(111) single-crystal substrate were studied by X-ray photoelectron diffraction (XPD), low-energy alkali ion scattering spectroscopy (ALISS), and low-energy electron diffraction (LEED). Alloying begins at temperatures above 500 K, and increasing the annealing temperature of deposited films to 900 K caused all Cu atoms to diffuse deep into the subsurface region of the Pt crystal. One particular Cu/Pt(111) bimetallic alloy surface was characterized in detail, and this surface was formed by depositing one monolayer of Cu onto the Pt(111) surface and then annealing to 550 K. Only a diffuse (1×1) LEED pattern was observed from this Cu/Pt(111) alloy, which indicates that there was no long-range, ordered intermetallic compound created at the surface for these conditions or any others that we investigated. ALISS and XPS were used to determine that the Cu concentration in the topmost, surface layer of this alloy was 7 atomic percent. XPD and ALISS give consistent results showing that Cu in this alloy was present in the first, second, and third layers at the surface, forming a surface alloy. Cu atoms in the alloy are located at Pt atom lattice sites, and are coplanar with the topmost Pt atomic layer without significant corrugation or buckling. Temperature programmed desorption (TPD) measurements showed that both CO and NO are more weakly adsorbed and have smaller desorption energies on the Cu/Pt(111) surface alloy compared to the Pt(111) surface.

© 2013 Elsevier B.V. All rights reserved.

1. Introduction

The structure and chemistry of Pt bimetallic surfaces are of fundamental interest because of the importance of Pt-based alloys as catalysts in the petrochemical industry. In particular, Cu/Pt catalysts have been investigated for their activity in oxidation of CO and hydrocarbons to CO_2 and water and hydrocarbon reforming reactions [1,2]. Cu is less active than Pt for these reactions, but Cu/Pt catalysts have a higher activity for both CO oxidation and hydrocarbon hydrogenolysis than pure Pt catalysts [2].

Previous work showed that ordered surface alloys can be created by the annealing of Sn films deposited on Pt single crystal substrates [3,4]. It is of interest to determine if similar ordered surface alloys can be created from Cu films deposited on Pt(111), as well as to compare the surface composition and structure of these Cu/Pt surface alloys with that of the bulk Cu–Pt alloy surfaces. From previous studies, it has been determined that the growth mode of Cu on Pt(111) is by a layer-by-layer mechanism at temperatures below 475 K [5–9]. Cu grows in islands within the first monolayer and these islands coalesce near monolayer coverage. No substrate reconstruction occurs during the growth of the Cu monolayer at a substrate temperature of 340 K [9]. The growth of a second layer only begins after the first Cu layer is complete. Cu/Pt surface alloys are formed at substrate temperatures above 500 K [5,6,8,10,11]. At temperatures from 500 to 1300 K, Cu diffuses from the surface into the bulk [6,8,10]; it was reported that all Cu had diffused deep into the bulk and no Cu AES signals were detected at 1250 K [8]. No Cu desorption was observed up to 1300 K [10], but around 1400 K, Cu atoms migrate back to the surface and desorb [8].

These observations can be compared to those from bulk phases, in which Cu and Pt form three ordered alloys or intermetallic compounds, *i.e.*, Cu_3Pt, CuPt, $CuPt_3$, at low temperatures and a disordered alloy at temperatures above 850 K [12]. Surface segregation in these alloys results in different surface and bulk compositions, for example the $Cu_3Pt(111)$ bulk alloy has an average composition of 75% Cu but has a surface composition of 80% Cu in the first layer and 69% Cu in the second layer after annealing at 850 K; this observation is in agreement with the higher surface energy of Pt (2.299 J/m^2) compared to Cu (1.952 J/m^2) [13]. LEED patterns suggest that these surface layers do not have long-range ordering [14,15].

We report herein on low energy electron diffraction (LEED), X-ray photoelectron diffraction (XPD) and low-energy alkali ion scattering spectroscopy (ALISS) studies of alloy surfaces formed by annealing Cu films deposited on Pt(111). These investigations included wide-ranging attempts to create long-range, ordered Pt-Cu surface alloys, as well as determination of the vertical displacement, if any, of Cu atoms

* Corresponding author. Tel.: +1 609 258 4524; fax: +1 609 258 0211.
E-mail address: bkoel@princeton.edu (B.E. Koel).

0039-6028/$ – see front matter © 2013 Elsevier B.V. All rights reserved.
http://dx.doi.org/10.1016/j.susc.2013.08.009

in the surface plane caused by the substitution of Cu atoms into the Pt crystal lattice. A linear relationship between the lattice mismatch and surface corrugation in a number of bimetallic surfaces with Sn alloyed into fcc(111) crystals has been observed, with the larger Sn atoms outwardly buckled in the vertical direction as a strain relief mechanism for the lattice mismatch [16–18]. The atomic radius of Cu (1.28 Å) is 8% smaller than that of Pt (1.39 Å) [5,6,9], and thus observation of any buckling of Cu atoms in the top Pt atomic layer would help determine the applicability of the empirical buckling relation beyond the previously studied Sn alloys. Moreover, identification of possible ordered Cu/Pt surface alloys would enable chemisorption and reaction studies of structure–reactivity relationships for the Cu–Pt bimetallic system.

Chemical characteristics of mixed and pure Cu/Pt surfaces have been modeled in using density-functional theory (DFT)[19–22]. Moreover, DFT has been used to examine catalyst function with respect to factors such as alloying, surface structure, adsorbate interactions, activity and selectivity [23,24]. Information about the structure and chemical activity of Cu/Pt surfaces is important for the verification and advancement of these models. This study presents a detailed characterization of the composition and structure of the prepared Cu/Pt surface as well as the NO and CO adsorption properties of the Cu/Pt bimetallic surface, similar to those carried out for other bimetallic Pt surface alloys [25–32].

2. Experimental methods

The two-level ultrahigh vacuum (UHV) chamber that was used had a base pressure in the low 10^{-10} Torr range and has been described in detail elsewhere [33]. The lower level housed a dual-anode Al/Mg Kα X-ray source for X-ray photoelectron spectroscopy (XPS) and XPD, Colutron ion gun to provide monoenergetic and collimated alkali or noble gas ions for low-energy ion scattering (LEIS) and ALISS, electron gun for Auger electron spectroscopy (AES), ion sputtering gun, and Perkin-Elmer Model 10-360 spherical capacitor analyzer (SCA) mounted at a fixed scattering angle θ of 144° for ALISS. Various ports were available for metal evaporators and gas dosers. The upper level was equipped with a 4-grid electron optics for LEED and UTI 100C quadrupole mass spectrometer (QMS) for temperature programmed desorption (TPD).

The manipulator was capable of two computer controlled rotational (azimuthal and polar planes) and three translational (*X*, *Y*, and *Z* axes) motions. The stepper motor precision during scanning of the polar angle (ψ or Ψ) and azimuthal angle ϕ for XPD and ALISS are ± 0.5° and ± 1°, respectively. Specification of the scattering angle θ in ALISS is accurate to ± 0.5°. The manipulator contained a sample holder that was capable of heating the crystal either resistively or by electron bombardment. The Pt(111) crystal (Atomergic Chemetals Corp.) was 10-mm diameter and 1.0-mm thick, and orientated to within ± 0.5°. It was mounted onto the sample stage by two 0.015-in W wires clamped to slots along the edge of the sample. The crystal temperature was monitored by a chromel/alumel thermocouple spot-welded to the edge of the crystal. The crystal was cleaned by repeated cycles of Ar^+-ion sputtering, heating in an O_2 background, and annealing in vacuum [27,32,34] until no contaminants were detected in XPS and a sharp (1 × 1) LEED pattern was observed.

The Cu doser was made by placing high purity Cu shot (ESPI, 6 N) inside of a Mo evaporation boat. Cu was deposited onto the Pt(111) surface by resistively heating the Mo boat and evaporation of Cu atoms through a pinhole in the boat cover. The evaporation temperature was measured by a chromel/alumel thermocouple spot welded to the center of the rear side of the Mo boat. Cu coverages were determined by CO TPD uptake curves from the Cu-covered Pt(111) surface [3,6,8]. In this report, the Cu coverage is defined relative to the Pt(111) surface atom density, so that Θ_{Cu} = 1 ML is 1.50 × 10^{15} atoms/cm^2.

In XPD studies, the polar angle ψ is defined with respect to the surface normal, with ψ = 0° corresponding to the analyzer perpendicular to the surface. The angle between the X-ray source and analyzer is fixed at 42.5°. An Al Kα X-ray source was used for both XPS and XPD scans. Pt and Cu signal intensities reported in XPD were obtained from integration of peak areas after subtracting an appropriate background. The X-ray source operating conditions and signal scan parameters were identical to those reported in ref. [32], except that the Cu $2p_{3/2}$ scan range was used from 925 to 945 eV BE.

According to convention in ALISS studies, the polar angle Ψ is defined with respect to the crystal surface, with Ψ = 90° corresponding to ions incident perpendicular to the surface. The angle between the energy analyzer and the incident ion beam is fixed at 36° for an ion scattering angle θ of 144°. The Na^+ ion source was a thermo ionic emitter using an aluminosilicate material which had been ion-exchanged using sodium ions. Measurements and analysis of ALISS spectra were similar to that in our previous Zn/Pt(111) study [32]. The operating conditions for the Na^+ ion source and the signal scan parameters were also identical to those reported in ref [32].

While a number of different surfaces produced by changing the deposition and annealing conditions were investigated, most of the characterization reported in this paper refer to the particular Cu/Pt(111) alloy surface created by depositing one monolayer of Cu onto Pt(111) at 300 K and subsequently annealing this surface to 550 K for 5 min.

3. Results and discussion

3.1. Evaluation of Cu coverages

CO adsorption was used as a probe of the amount of deposited Cu, as was used previously [6], and the results are shown in Fig. 1. The amount of adsorbed CO was determined from the integrated area under the CO desorption peak in TPD after exposing a saturation dose of CO to the Cu-covered Pt(111) surface at room temperature, and subsequently raising the substrate temperature to 500 K to desorb molecular CO from the surface. Within this temperature range, Cu atoms remain as adatoms at the Pt(111) surface and no alloying occurs [5,6,8,10,11]. The plot in Fig. 1 uses the Cu $2p_{3/2}$ intensity in XPS as the abscissa, measured after deposition of Cu on the Pt(111) surface at 300 K. The Cu $2p_{3/2}$ intensity was determined as the peak height in XPS after subtracting the background and normalization by the intensity of the Pt 4f peak from a clean Pt surface.

It is known that CO adsorbs only on Pt sites, and not on Cu sites, at temperatures above 230 K [6,35]. As Cu deposition increases,

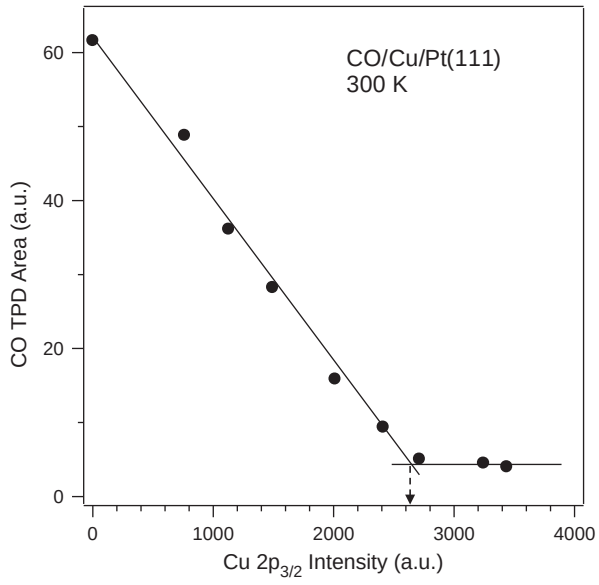

Fig. 1. Determination of the Cu monolayer coverage based on an evaluation of the CO TPD area as a function of the Cu $2p_{3/2}$ XPS intensity for Cu deposited on Pt(111) at 300 K. The arrow denotes 1-ML Cu.

corresponding to an increase in Cu $2p_{3/2}$ intensity, the CO TPD area decreases to and settles at a constant area slightly above zero indicating.

Cu monolayer coverage of the Pt(111) surface. The amount of CO adsorbed on the Cu-covered Pt(111) surface attenuates linearly with increasing Cu $2p_{3/2}$ intensity until the position indicated by the arrow that defines $\Theta_{Cu} = 1$ ML. The Cu$2p_{3/2}$ intensity associated with monolayer coverage was determined by the intersection of the two lines of best fit shown in Fig. 1; these are estimates and can vary depending on the way the best fit is drawn resulting in an uncertainty of ±5%. The CO TPD area does not go to zero even when much higher Cu coverages were used. Holst et al. [9] found holes in Cu films deposited on Pt(111) with a diameter of ~30 Å even after second layer Cu growth had started. The presence of these holes would make small areas of the Pt(111) substrate available for CO adsorption and thus account for the small amount of CO desorption in the experiments with more than 1 ML of Cu deposition. It is also possible that this non-zero value could be due to desorption of CO from edges of the Pt crystal [6].

3.2. LEED

We investigated a number of different Cu/Pt(111) alloy surfaces by depositing different amounts of Cu ($\Theta_{Cu} = 0.5$, 1, 3, and 5 ML) onto the Pt(111) surface at room temperature and subsequently annealing these samples to different temperatures from 550 to 900 K stepwise in increments of 50 K. For all of these surfaces, no new spots were observed in LEED except the original (1×1) pattern. In many cases the hexagonal (1×1) spots of these surface alloys were broader and lower in intensity than those of the clean Pt(111) surface. Thus, we never observed the reliable synthesis of any well-defined, long-range ordered alloy structures over this range of conditions.

3.3. Alloying process

For the particular case of one monolayer of Cu deposited on the Pt(111) surface at 300 K, we studied the alloying process using XPS and XPD. Fig. 2 shows how the Cu $2p_{3/2}$ intensity changed as the temperature was increased. The Cu signal was stable up to 500 K, but then decreased sharply prior to 550 K. Heating to 900 K nearly eliminated the Cu signal.

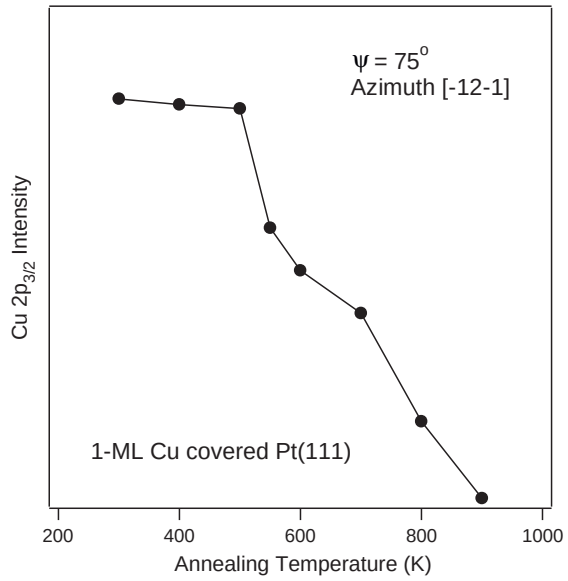

Fig. 2. Cu $2p_{3/2}$ XPS intensity for a 1-ML Cu film deposited on Pt(111) after annealing to several temperatures. The decrease in the Cu $2p_{3/2}$ intensity above 500 K indicates that alloying takes place at these high temperatures. Annealing at 900 K nearly eliminated the Cu signal, implying that Cu migrates deeply into the crystal.

Fig. 3 shows polar scans of the Cu $2p_{3/2}$ intensity along the [-12-1] azimuth obtained after annealing to selected temperatures. Following deposition and after annealing at temperatures up to 500 K, the Cu $2p_{3/2}$ peak in XPS was observed at every polar angle and there were no enhanced diffraction peaks such as those that would be observed if significant amounts of Cu were present in subsurface layers. This shows that Cu atoms were only present at the surface, either as adatoms or incorporated into the topmost layer only, with no alloying into subsurface layers. This is consistent with previous results reporting Cu alloying with Pt at temperatures higher than 500 K [5,6,8,10,11]. After annealing in the range of 550 to 800 K, the Cu $2p_{3/2}$ polar scans showed enhanced diffraction peaks that indicate diffusion of Cu atoms into the subsurface layers of the crystal to form an alloy, with Cu present in both the second and third layers in addition to the top layer. The angles stated in Figs. 3 and 4 were determined by calculations of the directions of high Pt-atom density chains from the known crystal lattice structure of Pt(111) and are used to look for and assign the observed diffraction peaks to specific atomic layers. The Cu $2p_{3/2}$ peak had the same intensity at every polar angle and any enhanced diffraction features in the polar scans were eliminated following annealing at 900 K. This indicates that there is no appreciable amount of Cu present in either the second or third layers, and most of the Cu atoms have diffused deep into the bulk of the crystal. This behavior is consistent with previous reports [6,8,10].

In the remainder of this paper, additional characterization was carried out for the particular Cu/Pt(111) bimetallic alloy formed by depositing one monolayer of Cu onto the Pt(111) surface at 300 K and subsequently annealing at 550 K. This surface showed only the (1×1) spots of Pt(111) in LEED, as described above. Quantitative

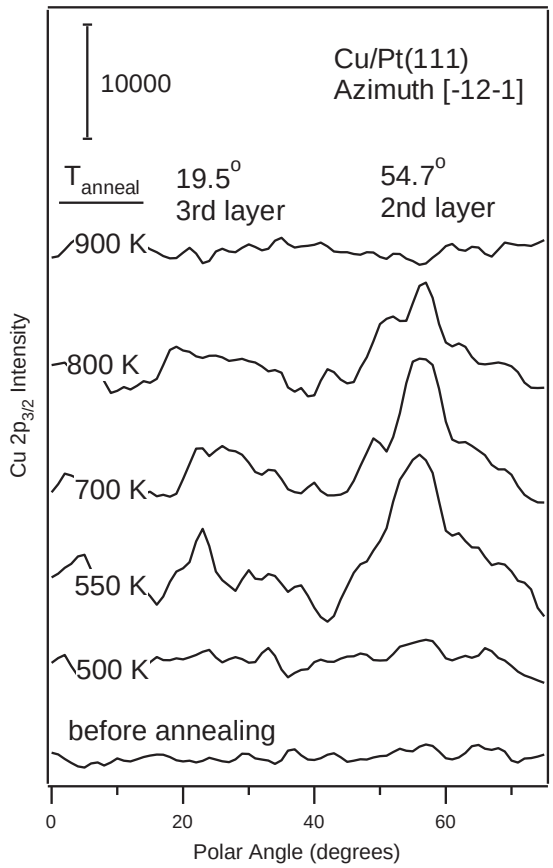

Fig. 3. XPD polar scans of the Cu $2p_{3/2}$ intensity of 1-ML Cu deposited on Pt(111) over polar angles of $\psi = 0°$ to 75° along the [-12-1] azimuthal direction after annealing. The enhanced Cu $2p_{3/2}$ diffraction features were observed after annealing at 550 K, indicating that alloying occurs at this temperature. Angle labels above the curves are predicted enhancement directions based on the known structure of Pt(111).

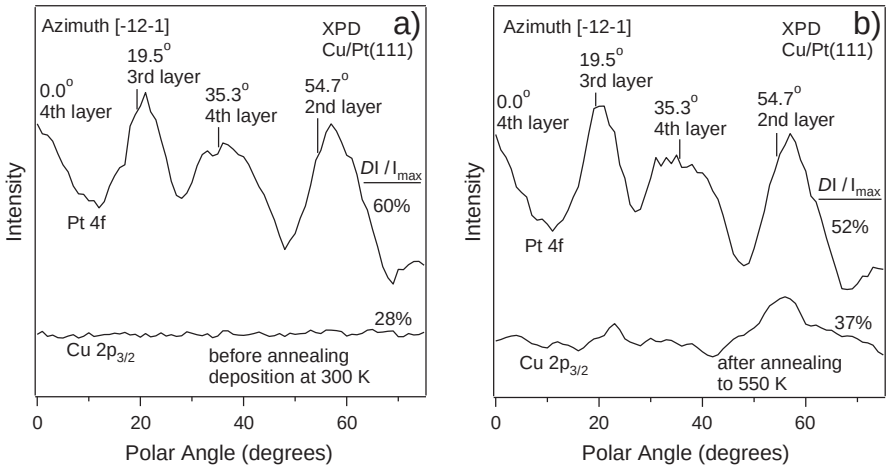

Fig. 4. (a) XPD polar scans along the [-12-1] azimuth for 1-ML Cu deposited on Pt(111) at 300 K before annealing. (b) XPD polar scans along the [-12-1] azimuth for 1-ML Cu deposited on Pt(111) at 300 K after annealing at 550 K and forming a Cu–Pt alloy. Angle labels above the curves are predicted enhancement directions based on the known structure of Pt(111).

analysis of the Cu concentration in the topmost (surface) layer of this surface alloy was determined by ALISS and estimated by XPS. As presented below, this concentration was found to be 7.2 at. %, or $\Theta_{Cu} = 0.072$ ML.

3.4. XPD

Fig. 4(a) shows XPD polar scans along the [-12-1] azimuthal direction following deposition of 1-ML Cu on the Pt(111) surface at 300 K. Polar scans of the Pt 4f (summing both $4f_{7/2}$ and $4f_{5/2}$ contributions) intensity had four forward-scattering features close to the angles $\psi = 0°$, 19.5°, 35.3°, and 54.7° corresponding to the expected, specific internuclear directions due to Pt atoms in the 4th, 3rd, 4th, and 2nd-layers, respectively [32]. The Cu $2p_{3/2}$ polar scan, on the other hand, showed no preferred emission angle and the Cu $2p_{3/2}$ peak was observed in XPS at every polar angle. As discussed above, this indicates that the deposited Cu atoms remain only at the surface.

Annealing at 550 K causes alloying and Cu diffusion into the 2nd-and 3rd-layers. XPD polar scans for Pt and Cu along the [-12-1] azimuth for this alloy are shown in Fig. 4(b). The Pt 4f polar scan was same as the scan before annealing, consistent with most Pt atoms remaining at positions that are unchanged from the bulk termination on clean Pt(111). For the Cu $2p_{3/2}$ polar scans, enhanced diffraction peaks now appear near $\psi = 19.5°$ and 54.7°, which establishes that Cu atoms are incorporated into the 2nd- and to some extent the 3rd-subsurface layers. The loss in Cu intensity in XPS comes from the migration of most Cu atoms into the bulk of the crystal rather than Cu desorption from the surface [6,8,10].

3.5. ALISS

Fig. 5 displays polar angle scans for 1-keV Na^+ ions scattered from the clean Pt(111) surface along [-12-1], [-211], [-110] azimuths, respectively. No Pt scattering signal is observed at low polar angles, because all of the surface atoms are hidden inside the shadow cones created by their preceding neighbor when the polar angle Ψ is sufficiently low [36,37]. As the polar angle increases, first-layer atoms emerge out of the shadow cones at a critical angle Ψ_c. Along the long azimuths [-12-1] and [-211], this gives rise to the peak near 20°. The peaks near 57° along the [-12-1] azimuth and 87° along the [-211] azimuth arise from the emergence of 2nd and 3rd-layer Pt atoms, respectively, from the shadow cones of the top-layer Pt atoms [14,18,32]. Along the short azimuth [-110], the peak from first-layer Pt atoms is near 29°, which is at higher polar angle than that of the long azimuthal direction (near 20°). This is because the interatomic distance along the short azimuthal direction ([-110]) is smaller than that along the long azimuthal direction ([-12-1] or [-211]), and thus a higher polar angle is needed along the short azimuth to bring the first-layer Pt atoms out of the shadow cones created by their preceding neighbors [3,18,32].

Polar scans for 1-keV Na^+ ions scattered from Pt atoms in the Cu/Pt(111) alloy along the [-12-1], [-211], and [-110] azimuthal directions are shown in Fig. 6. Along all three azimuths, the scattering features are similar in profile and peak position to that of clean Pt(111) shown in Fig. 5. If Cu adatoms formed an overlayer on the Pt surface, the Pt first-layer critical angle of the surface alloy should be much larger than that of clean Pt(111). Therefore, this establishes that Cu atoms are incorporated into the first Pt layer to form an alloy.

There is the possibility that because the concentration of Cu at the surface is small, even if Cu formed an overlayer, the Pt first-layer scattering feature would not be shifted appreciably to higher polar angles. This is because most of the Pt atoms are still surrounded by other Pt atoms rather than Cu atoms. Later, we will use the Cu polar angle scans from the Cu/Pt(111) alloy to further determine the location of Cu atoms at this surface.

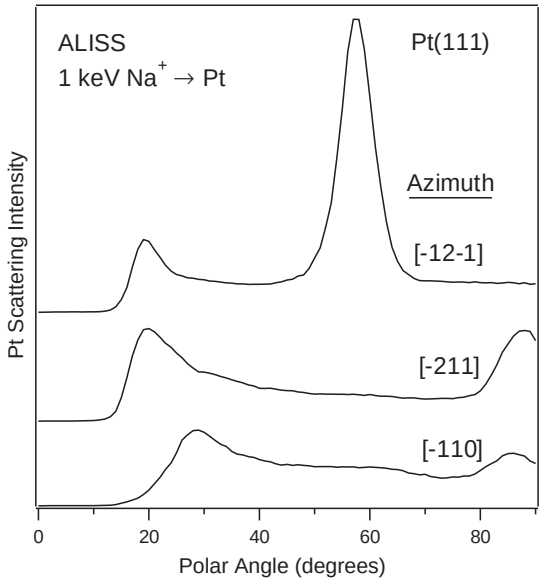

Fig. 5. Polar angle scans for 1-keV Na^+ ions scattered from the clean Pt(111) surface along the [-12-1], [-211], and [-110] azimuthal directions, respectively.

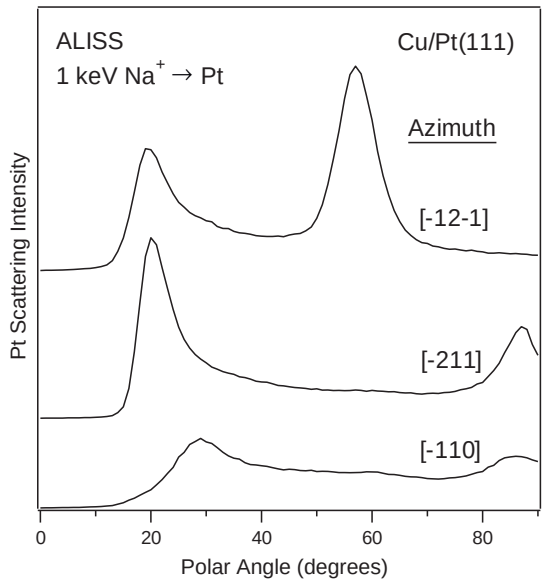

Fig. 6. Polar angle scans for 1-keV Na^+ ions scattered from Pt atoms for the Cu/Pt(111) alloy along the [-12-1], [-211], and [-110] azimuthal directions, respectively.

Fig. 7 shows polar angle scans for 1-keV Na^+ ions scattered from Cu atoms in the Cu/Pt(111) alloy along the [-12-1], [-211], and [-110] azimuths, respectively. The curve along the [-12-1] azimuth has a profile and peak positions similar to the Pt scattering features for both clean Pt(111) and the Cu/Pt(111) alloy, as presented in Figs. 5 and 6. Peaks were observed near $\Psi = 20°$ and 57° that are attributed to scattering from 1st and 2nd-layer Cu atoms, respectively. If Cu atoms formed an overlayer, the first-layer Cu peak should be at much lower polar angle than those of the first-layer Pt peaks at 20°. Furthermore, because the Cu/Pt(111) surface alloy has a dilute Cu concentration, the spacing between a Cu adatom and its nearest neighbor Cu adatom would be very large. Therefore, if Cu atoms were present as an overlayer, the enhanced, first-layer Cu scattering feature should be located at a much lower angle

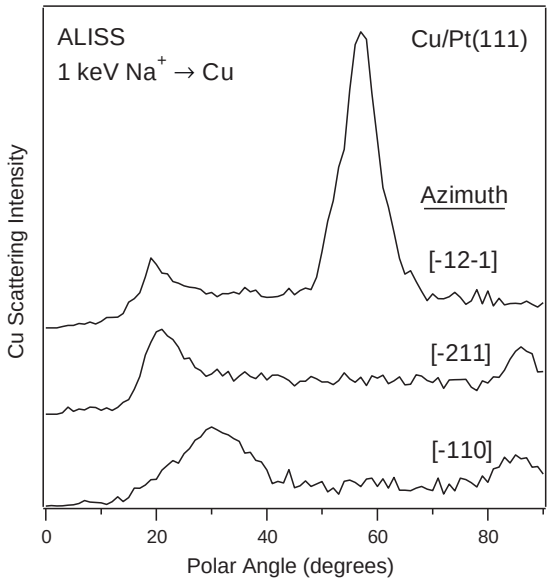

Fig. 7. Polar angle scans for 1-keV Na^+ ions scattered from Cu atoms for the Cu/Pt(111) alloy along three different directions, the long azimuths [-12-1], [-211], and the short azimuth [-110]. The observed enhanced scattering features contain contributions from 1st, 2nd, and 3rd-layer Cu atoms.

than observed. This occurs because most Cu adatoms would be visible outside of the shadow cones created by the nearest preceding Cu adatoms even at a very low polar angle. In contrast to this situation, the first-layer scattering features in both Cu and Pt scans have the same peak positions. Therefore, these scans show that Cu atoms are substitutionally incorporated into the topmost layer of Pt atoms rather than form an overlayer. In addition, an enhanced second-layer Cu scattering feature at around 57° is observed along the [-12-1] azimuthal direction. This establishes that Cu atoms also occupy second-layer Pt sites in this alloy. This is consistent with the conclusion obtained from the Cu $2p_{3/2}$ XPD polar scan shown in Fig. 4(b).

Along the [-211] azimuth, the Cu scattering features also are similar in profile and peak positions to those from Pt scattering in clean Pt(111) and the Cu/Pt(111) alloy shown in Figs. 5 and 6. Peaks near $\Psi = 20°$ and 87° contain contributions from scattering by 1st and 3rd-layer atoms, respectively. By the same reasoning given for scans along the [-12-1] direction, this result shows that Cu atoms replace the topmost-layer Pt atoms by incorporation to form an alloy rather than an overlayer. Cu scattering along the [-211] azimuth has a 3rd-layer scattering feature near 87° which is similar to that observed in Pt scattering from clean Pt(111) and the Cu/Pt(111) alloy. This shows that Cu alloys with Pt in the third layer too, consistent with the results from Cu $2p_{3/2}$ XPD polar scans shown in Fig. 4(b). Cu enhanced scattering features along the [-110] short azimuthal direction are completely consistent with these conclusions. In summary, ALISS establishes that there is a substantial concentration of Cu atoms in the top three Pt layers, forming a bimetallic alloy, after heating 1-ML Cu on the Pt(111) surface to 550 K.

The ALISS data can also be used to quantitatively determine the Cu concentration in the topmost layer of the alloy. This is accomplished by using the 1st layer scattering intensity where there is little dependence of intensity on angle; $\Psi = 55°$ along the [-211] azimuth, was used in this study. Thus, the Cu concentration can be determined using the ion scattering intensities measured for Cu and Pt at this angle for the Cu/Pt(111) alloy and the following relationship:

$$C_{Cu} = \frac{I_{Cu}/S_{Cu}}{I_{Cu}/S_{Cu} + I_{Pt}/S_{Pt}} \quad (1)$$

The sensitivity factors were evaluated using ALISS spectra taken at the same conditions for clean Pt(111) and a thick Cu film (where no Pt scattering was observed). This determined that $S_{Pt}/S_{Cu} = 1.12$, and that $C_{Cu} = 0.07 \pm 0.01$ ML (this uncertainty is based on the reproducibility of the scattering intensities).

Quantitative analysis by XPS gave a consistent answer for the Cu concentration in this alloy. The Cu XPS signal was directly compared to the Ge XPS signal obtained for the $(\sqrt{19} \times \sqrt{19})$R23.4°-Ge/Pt(111) surface alloy which contains 0.053-ML Ge in the top layer [31]. Using the tabulated relative sensitivity factors for Cu and Ge in XPS [38], the composition of Cu at the surface was determined to be quite dilute, about 7%, in good agreement with the ALISS determination.

3.6. Critical angles in ALISS and the buckling distance

The relative vertical position between Cu and Pt atoms in the top layer can be calculated from their corresponding critical angles Ψ_c [3,4,14–18]; by convention Ψ_c is the angle where the scattering intensity is 90% of the maximum intensity of the enhanced scattering peak [4,16,18]. The first-layer enhanced scattering features for Pt scattering (from clean Pt(111) and the Cu/Pt(111) alloy) and Cu scattering (from the Cu/Pt(111) alloy) along the [-12-1] azimuthal direction are shown in Fig. 8. The critical angles Ψ_c are labeled and assigned at 18.2°, 18.3°, and 18.6° for each scan, respectively. The Pt scattering peaks from clean Pt(111) and the Cu/Pt(111) alloy have almost the same critical angles. This implies that the average position of first-layer Cu atoms is coplanar with Pt atoms in the Pt(111) surface layer without appreciable "buckling", or vertical displacement, observed.

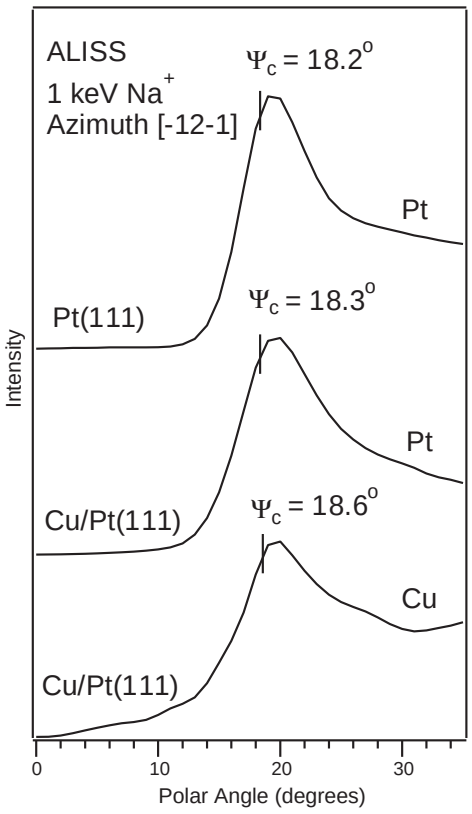

Fig. 8. Polar scans of first-layer scattering features for Pt (from clean Pt(111) and the Cu/Pt(111) alloy) and Cu (from the Cu/Pt(111) alloy) along the [-12-1] azimuthal direction. The position of each critical angle Ψ_c is marked by a short bar.

Nevertheless, we cannot dismiss the possibility that the dilute concentration of Cu at the surface does not substantially alter the Pt critical angle. Most Pt atoms at the surface are still surrounded by other Pt atoms rather than Cu atoms, and relatively few Pt atoms have a Cu atom neighbor along a particular direction.

Cu scattering features are more informative about the corrugation of Cu atoms at the alloy surface. Because of the low concentration of Cu in the alloy, most Cu atoms are surrounded by Pt rather than Cu atoms. If there is significant buckling of Cu atoms within the Pt surface plane, either inward or outward, there will be a shift of the critical angle position for the Cu scattering peak. The critical angle of the first-layer Cu scattering peak at 18.6° is very close to that of the first-layer Pt scattering peak at 18.3°. This establishes that there is no significant buckling of Cu either out of or into the top Pt layer. A shift of more than 1° in the critical angle would be caused by only a 0.05 Å displacement in vertical position for the Cu–Pt bimetallic system [15]. This, and data from the other two azimuthal directions, [-211] and [-110], show that there is no appreciable (<0.02 Å) corrugation of Cu atoms at the surface. Similar results using ALISS were obtained on a bulk, Cu_3Pt alloy single-crystal showing no significant buckling of Cu or Pt [14,15].

Previously, a linear empirical relationship between the lattice mismatch and surface corrugation in a number of bimetallic surfaces with Sn alloyed into *fcc*(111) crystals was observed [16–18]. In these surfaces, an outward buckling of the larger Sn atoms in the vertical direction was induced. The current study shows that substituted Cu atoms are coplanar with Pt in the Pt(111) surface as was observed for bulk Cu_3Pt single crystals [14,15]. This observation shows that the empirical buckling relationship does not apply for substitutional atoms smaller than those of the host crystal and the correlation cannot be extended from Sn–Pt alloys to the Cu–Pt system.

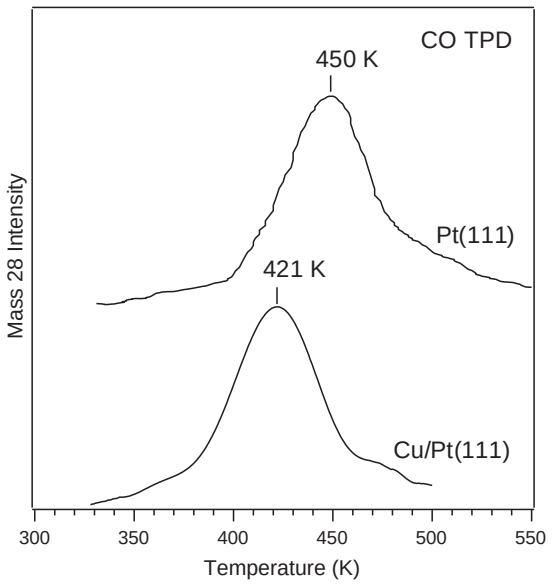

Fig. 9. CO TPD spectra from clean Pt(111) and the Cu/Pt(111) alloy surface after a 0.05 L CO exposure at room temperature.

3.7. TPD

CO TPD spectra from Pt(111) and the Cu/Pt(111) alloy ($\Theta_{Cu} = 0.072$ ML) are shown in Fig. 9. The same low exposure of 0.05-L CO was dosed to these surfaces at 325 K. At this temperature, CO adsorbs exclusively at Pt sites [6,35]. For the Cu/Pt(111) alloy, CO TPD was monitored to 500 K, where Cu still remains on the surface rather than diffusing into the substrate [6,8,10]. The desorption peak for low coverages of CO on Pt(111) near 450 K is assigned to CO that desorbs from Pt atop sites [25,39,40]. When Cu alloys with Pt, CO desorbs from Pt at lower desorption temperatures in a peak near 421 K. This decrease in the desorption energy of CO from Pt sites at the surface of the Cu/Pt(111) alloy was attributed previously to the change in electronic structure of Pt that is induced by alloying with Cu [6,35].

DFT calculations comparing CO bonding on Pt(111) and Cu_3Pt(111) have shown that the adsorption energy of CO on Cu_3Pt(111) is

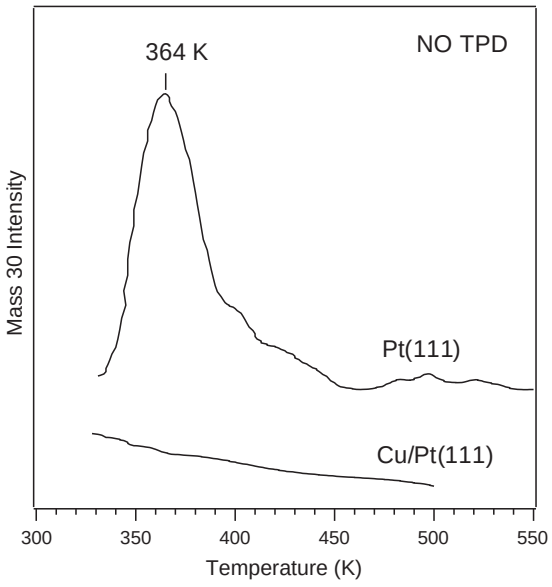

Fig. 10. NO TPD spectra from clean Pt(111) and the Cu/Pt(111) alloy surface after a 3 L NO exposure at room temperature.

decreased compared to that on Pt(111) [19,43]. Zhang et al. attributed this to a small shift of 0.1 eV towards higher energies in the local density of states (LDOS) [43] and Hammer et al. [19] noted a shift in the CO 5σ level due to these changes. Furthermore, HREELS studies by Becker et al. found significant weakening of the Pt–CO bond for $Cu_3Pt(111)$ compared to that on Pt(111) [44].

NO TPD traces from Pt(111) and the Cu/Pt(111) alloy surface are shown in Fig. 10. These surfaces were each exposed to 3-L NO, which gives a saturation coverage of NO on Pt(111) at 325 K. The NO desorption peak on Pt(111) at 364 K has been assigned to desorption of NO from bridge sites [26,41,42]. After Cu was alloyed with Pt, no NO desorption was observed in TPD. This implies that alloying caused a reduction in the NO desorption temperature to below room temperature resulting in no NO adsorbed on the Cu/Pt alloy surface under these conditions. We found no reports for DFT studies of NO adsorption on Cu–Pt systems that we could use to compare with our results.

4. Conclusions

We have explored aspects of the use of Cu deposition on a Pt(111) single crystal for creating Cu/Pt(111) bimetallic alloy surfaces. Different amounts of Cu between 0.5 and 5 ML were deposited onto the Pt(111) surface and annealed at various temperatures ranging from 550 to 900 K. LEED observations during this processing never revealed new spots indicative of an ordered alloy structure. For one particular Cu/Pt(111) alloy surface, *i.e.*, that formed by depositing one monolayer of Cu onto Pt(111) and subsequently annealing at 550 K, we carried out additional XPD and ALISS investigations of the structure. Cu adatoms begin to be incorporated into the surface and form an alloy at annealing temperatures higher than 500 K. The Cu concentration of this alloy is about 7.2%, as determined by quantitative analysis using ALISS and XPS. XPD and ALISS results are consistent with each other and show that Cu in this alloy is present in the topmost, second, and third atomic layers of the crystal. These alloyed Cu atoms are incorporated substitutionally into Pt lattice sites in each layer at positions very close to the same as those of the replaced Pt atoms. In particular, Cu atoms present at the surface occupy sites without appreciable buckling ($\lesssim$0.02 Å). Previous observations of a linear relationship between the lattice mismatch and surface corrugation in a number of bimetallic surfaces with Sn alloyed into *fcc*(111) crystals, where an outward buckling of the larger Sn atoms in the vertical direction was induced, cannot be extended to this system. When the annealing temperature was increased to 900 K, all Cu atoms migrated deeply into the subsurface of the crystal. CO, and especially NO, bonds more weakly on the Cu/Pt(111) alloy surface prepared in this work compared to that on the clean Pt(111) surface, and this is consistent with previous studies using other Cu/Pt alloy surfaces.

Acknowledgment

BEK acknowledges that this material is based upon work supported by the National Science Foundation under Grant No. CHE-1129417.

References

[1] J.T. Kummer, J. Catal. 38 (1975) 166.
[2] H.C. De Jongste, V. Ponec, J. Catal. 63 (1980) 389.
[3] S.H. Overbury, D.R. Mullins, M.T. Paffett, B.E. Koel, Surf. Sci. 254 (1991) 45.
[4] Y. Li, B.E. Koel, Surf. Sci. 330 (1995) 193.
[5] M.T. Paffett, C.T. Campbell, T.N. Taylor, S. Srinivasan, Surf. Sci. 154 (1985) 284.
[6] R.C. Yeates, G.A. Somorjai, Surf. Sci. 134 (1983) 729.
[7] M. Shek, P. Stefan, I. Lindau, W. Spicer, Phys. Rev. B 27 (1983) 7277.
[8] J.A. Rodriguez, C.M. Truong, D.W. Goodman, J. Chem. Phys. 96 (1992) 7814.
[9] B. Holst, M. Nohlen, K. Wandelt, W. Allison, Surf. Sci. 377–379 (1997) 891.
[10] M. Kuhn, J.A. Rodriguez, J. Vac. Sci. Technol. A 13 (1995) 1569.
[11] M. Kuhn, J.A. Rodriguez, Catal. Lett. 32 (1995) 345.
[12] M. Hansen, K. Anderko, Constitution of Binary Alloys, 2nd ed. McGraw-Hill, 1958.
[13] L. Vitos, A.V. Ruban, H.L. Skriver, J. Kollar, Surf. Sci. 411 (1998) 186.
[14] Y.G. Shen, D.J. O'Connor, K. Wandelt, R.J. MacDonald, Surf. Sci. 328 (1995) 21.
[15] Y.G. Shen, D.J. O'Connor, R.J. MacDonald, K. Wandelt, Solid State Commun. 96 (1995) 557.
[16] Y. Li, M. Voss, N. Swami, Y.-L. Tsai, B. Koel, Phys. Rev. B 56 (1997) 15982.
[17] S. Overbury, Y.-S. Ku, Phys. Rev. B 46 (1992) 7868.
[18] Y.-S. Ku, S.H. Overbury, Surf. Sci. 273 (1992) 341.
[19] B. Hammer, Y. Morikawa, J.K. Nørskov, Phys. Rev. Lett. 76 (1996) 2141.
[20] P.J. Feibelman, B. Hammer, J.K. Nørskov, F. Wagner, M. Scheffler, R. Stumpf, R. Watwe, J. Dumesic, J. Phys. Chem. B 105 (2001) 4018.
[21] J.R. Kitchin, J.K. Nørskov, M.A. Barteau, J.G. Chen, J. Chem. Phys. 120 (2004) 10240.
[22] B. Hammer, J.K. Nørskov, Surf. Sci. 343 (1995) 211.
[23] B. Hammer, J.K. Nørskov, Adv. Catal. 45 (2000) 71.
[24] J.K. Nørskov, T. Bligaard, J. Rossmeisl, C.H. Christensen, Nat. Chem. 1 (2009) 37.
[25] M.T. Paffett, S.C. Gebhard, R.G. Windham, B.E. Koel, J. Phys. Chem. 94 (1990) 6831.
[26] C. Xu, B.E. Koel, Surf. Sci. 310 (1994) 198.
[27] Y.L. Tsai, B.E. Koel, J. Phys. Chem. B 310 (1–3) (1994) 198–208.
[28] J.W. Peck, D.I. Mahon, D.E. Beck, B.E. Koel, Surf. Sci. 410 (1998) 170.
[29] C. Panja, B.E. Koel, J. Phys. Chem. A 104 (2000) 2486.
[30] C. Panja, N.A. Saliba, B.E. Koel, Catal. Lett. 68 (2000) 175.
[31] C.-S. Ho, S. Banerjee, M. Batzill, D.E. Beck, B.E. Koel, Surf. Sci. 603 (2009) 1161.
[32] C.-S. Ho, E. Martono, S. Banerjee, J. Roszell, J. Vohs, B. Koel, J. Phys. Chem. A (2013), http://dx.doi.org/10.1021/jp4006668, (accepted for publication).
[33] C.S. Ho, S. Banerjee, B.E. Koel, O.B. Duchemin, J.E. Polk, Appl. Surf. Sci. 252 (2006) 2657.
[34] R.G. Musket, W. McLean, C.A. Colmenares, D.M. Makowiecki, W.J. Siekhaus, Appl. Surf. Sci. 10 (1982) 143.
[35] U. Schneider, G.R. Castro, K. Wandelt, Surf. Sci. 287–288 (1993) 146.
[36] H. Niehus, W. Heiland, E. Taglauer, Surf. Sci. Rep. 17 (1993) 213.
[37] D.P. Woodruff, T.A. Delchar, Modern Techniques of Surface Science, 2nd ed. Cambridge University Press, Cambridge, 1994.
[38] J.F. Moulder, W.F. Stickle, P.E. Sobol, K.D. Bomben, Handbook of X-Ray Photoelectron Spectroscopy, Perkin-Elmer Corporation, Eden Prairie, 1992.
[39] P.R. Norton, J.W. Goodale, E.B. Selkirk, Surf. Sci. 83 (1979) 189.
[40] H. Steininger, S. Lehwald, H. Ibach, Surf. Sci. 123 (1982) 264.
[41] B.E. Hayden, Surf. Sci. 131 (1983) 419.
[42] M.E. Bartram, B.E. Koel, E.A. Carter, Surf. Sci. 219 (1989) 467.
[43] C.H. Zhang, R.J. Baxter, A. Alavi, M.H. Lee, J. Chem. Phys. 115 (2001) 5272.
[44] C. Becker, T. Pelster, M. Tanemura, J. Breitbach, K. Wandelt, Surf. Sci. 427–428 (1999) 403.